WARWICK
THE UNIVERSITY OF WARWICK

Manuscript version: Author's Accepted Manuscript
The version presented in WRAP is the author's accepted manuscript and may differ from the published version or Version of Record.

Persistent WRAP URL:
http://wrap.warwick.ac.uk/150272

How to cite:
Please refer to published version for the most recent bibliographic citation information. If a published version is known of, the repository item page linked to above, will contain details on accessing it.

Copyright and reuse:
The Warwick Research Archive Portal (WRAP) makes this work by researchers of the University of Warwick available open access under the following conditions.

Copyright © and all moral rights to the version of the paper presented here belong to the individual author(s) and/or other copyright owners. To the extent reasonable and practicable the material made available in WRAP has been checked for eligibility before being made available.

Copies of full items can be used for personal research or study, educational, or not-for-profit purposes without prior permission or charge. Provided that the authors, title and full bibliographic details are credited, a hyperlink and/or URL is given for the original metadata page and the content is not changed in any way.

Publisher's statement:
Please refer to the repository item page, publisher's statement section, for further information.

For more information, please contact the WRAP Team at: wrap@warwick.ac.uk.

warwick.ac.uk/lib-publications

Journal Name

ARTICLE TYPE

Cite this: DOI: 10.1039/xxxxxxxxxx

Can we use on-the-fly quantum simulations to connect molecular structure and sunscreen action?†

Gareth W. Richings, Christopher Robertson, and Scott Habershon[a]

Received Date
Accepted Date

DOI: 10.1039/xxxxxxxxxx

www.rsc.org/journalname

The ground-up design of new molecular sunscreens, with improved photostability, absorbance and spectral coverage, stands as a challenge to fundamental chemical science. Correlating sunscreen molecular structure and function requires detailed insight into the relaxation pathways available following photoexcitation; however, the complex coupled electron/nuclear dynamics in these systems stands as a tough challenge to computational chemistry. To address this challenge, we have recently developed efficient and accurate simulation methods to model non-adiabatic dynamics of general molecular systems as a route to correlating photoinduced dynamics and potential sunscreen activity. Our approach, combining the multi-configuration time-dependent Hartree (MCTDH) method with PESs generated using machine-learning, represents a new "on the fly" strategy for accurate wavefunction propagation, with the potential to provide a new "black box" strategy for interrogating ultrafast dynamics in general photoinduced energy transport processes. Here, we illustrate our attempts to apply this methodology to study the ultrafast photochemistry of four compounds derived from mycosporine-like amino acids (MAAs), compounds which are believed to act as microbial sunscreens in micro-organisms such as algae. Specifically, we investigate how the choice of active vibrational space and diabatic electronic states in MCTDH strongly influences the predictions of ultrafast dynamic relaxation in representative MAAs. Our results serve to demonstrate that "on the fly" quantum dynamics using MCTDH is increasingly viable, but important barriers relating to coordinate choices and diabatisation remain.

1 Introduction

The direct solution of the time-dependent Schrödinger equation (TDSE) can provide a wavefunction describing the electronic and nuclear motion in a molecular system undergoing either adiabatic or non-adiabatic dynamics. As such, wavefunction propagation simulations are an invaluable tool for interrogating ultrafast (*i.e.* a few hundred fs) chemical dynamics in molecular systems, with applications including calculation of absorption and emission spectra, determination of reactive fluxes, prediction of reaction mechanisms, and prediction of non-linear or multidimensional spectroscopies.

Among the wide range of methods proposed for propagating wavefunctions using the TDSE, the multi-configuration time-dependent Hartree (MCTDH) method occupies a central position.[1–3] In MCTDH, the time-dependent wavefunction is written as a completely general tensor product of basis functions (termed single-particle functions [SPFs] in MCTDH) for each degree-of-freedom, with each Hartree product of SPFs being associated with a complex expansion coefficient. In MCTDH, both the SPFs and the expansion coefficients are time-dependent, and the Dirac-Frenkel variational principle is used to derive equations-of-motion which are propagated to produce a time-dependent wavefunction. To date, MCTDH (and extensions such as multi-layer MCTDH,[4–6] aimed at treating systems with greater numbers of degrees-of-freedom) has been used to study an enormous range of molecular chemistry, with representative examples including non-adiabatic dynamics in organic molecules such as pyrazine,[7–9] pyrroles[10] and DNA bases,[11] to complex materials such as dye chromophores adsorbed on TiO_2 nanoparticles[12,13] or spin-orbit coupling in organometallic complexes.[14]

However, a key computational drawback of MCTDH has played an important role in preventing wider uptake of this powerful approach; in particular, for efficient numerical implementation, MCTDH requires that the potential energy surface (PES) of the molecular system of interest be available in the form of a *sum-of-products*. While one can always fit a PES with a functional form of the appropriate sum-of-products structure required for

[a] *Department of Chemistry and Centre for Scientific Computing, University of Warwick, Coventry, CV4 7AL, United Kingdom. E-mail: S.Habershon@Warwick.ac.uk*

† Electronic Supplementary Information (ESI) available. See DOI: 10.1039/b000000x/

This journal is © The Royal Society of Chemistry [year]

efficient MCTDH simulations,[15–18] this fitting process can itself be cumbersome and inaccurate; for example, while approximate models such as the vibronic coupling Hamiltonian are useful in describing small-amplitude molecular dynamics, more complex processes, such as hydrogen dissociation, can be difficult to describe correctly. In addition, fitting sum-of-products PES forms to *ab initio* data can itself present challenges, notably in the choice of reference data. Technically, MCTDH requires a *global* PES describing all accessible molecular geometries which might feature in a wavefunction propagation simulation; however, this requirement is contrary to the *local* nature of *ab initio* electronic structure calculations.

In our recent work,[19–22] we have made a number of contributions which are aimed at implementing an "on-the-fly" or "direct" MCTDH simulation strategy. We have shown how one can construct both adiabatic and non-adiabatic PESs describing complex chemical systems during the course of an MCTDH wavefunction propagation, in contrast to the standard approach of fitting a global PES *prior* to propagation. Our approach, described below, uses kernel ridge regression (KRR) to automatically generate a simple functional representation of the PES upon which the MCTDH wavefunction is evolving,[23] in a similar manner to the GROW methodology proposed by Collins and co-workers.[24,25] Combined with an additional two-body or three-body decomposition of the resulting KRR PES, our scheme enables automatic generation of a PES in tandem with wavefunction propagation, providing an overall wavefunction propagation method which does not require pre-fitting of a global PES. Our direct-dynamics MCTDH (DD-MCTDH) scheme offers a new computational tool for modelling quantum chemical dynamics while circumventing some of the computational roadblocks which have stood in the way of direct implementations of MCTDH in the past.

One particularly important emerging application domain for direct quantum dynamics simulations is the design of new molecular sunscreens.[26–29] With increasing prevalence of health issues arising from over-exposure to the sun, notably melanoma and other cancers, as well as increased awareness of the dangers of sun exposure, there is a globally growing demand to develop molecular sunscreens which outperform current market products in regards to higher UVA (315 - 400 nm) or UVB (280-315 nm) absorption strength, minimal photoproduct formation, maximal photostability and low risk of photosensitization or allergy. However, the *de novo* design of new organic sunscreen molecules is hampered because the molecular mechanism of action of many sunscreen filters is simply not well enough understood at the molecular level; while general principles regarding the desired properties of sunscreens, such as strong UVA/UVB absorption, photostability and absence of toxic photoproducts, are clearly defined, the connection between molecular structure, electronic state manifolds and photodynamic relaxation in governing the ultimate efficiency of molecular sunscreens remains difficult to predict.

In this paper, we present the first application of our DD-MCTDH scheme to directly investigate the correlation between molecular electronic structure, molecular quantum photodynamics, and emergent sunscreen potential. In particular, we investigate the photodynamics in four different organic molecules which are derived from a category of natural products known as mycosporine-like amino acids (MAAs; Fig. 1). MAAs comprise a core moiety of either a cyclohexenone or cyclohexenimine with a variety of peripheral functional groups (typically alcohols or carboxylic acids).[30,31] These molecules are commonly found in high-UV natural environments, and have been discovered in microbes, algae and fungi; MAAs are strongly associated with a function as microbial sunscreens, with the expectation that the cyclic conjugated core structure acts as a strong UV absorber. In addition to their absorption properties, MAAs exhibit a high degree of photostability, as well as other desirable properties for sunscreen formulations, such as water solubility.

In a recent experimental and computational study of sunscreen performance for MAAs, Losantos and co-workers used a series of quantum chemical calculations for several MAA-like compounds, as well as direct synthesis and absorption spectra characterization, in an attempt to rationally-design molecular compounds with improved sunscreen action.[28] Excited-state minimum energy path (MEP) calculations for 1a and 3a suggested that 3a is a better sunscreen candidate than 1a, with a first excited-state (S_1) PES which leads to fast relaxation to the S_0 ground-state through a conical intersection. This conclusion is supported by non-adiabatic trajectory surface-hopping simulations of 3a, which illustrated ultrafast relaxation to the ground-state in around 200 fs. Building on these studies of 3a, this prior work then proposed a number of modified molecular structures in the search for improved sunscreen function building on the structure of 3a, with promising sun-protection factors measured for formulations containing five-membered ionic compounds which are analogous to the cyclohexenimine core.

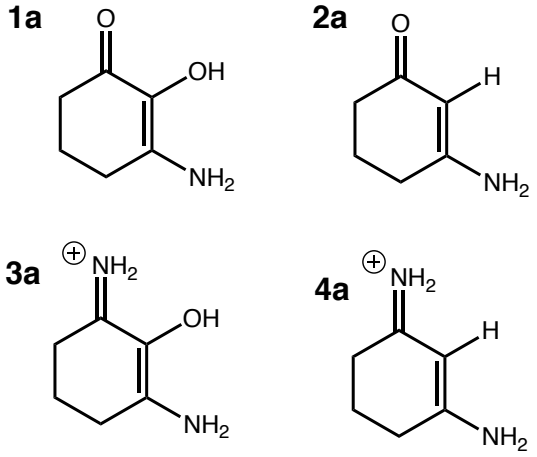

Fig. 1 MAA analogue structures studied here. Structures **1a**-**4a** are closely related to MAAs which have been studied previously by experiment and surface-hopping simulations; the only difference, as noted below, is that methyl groups on the amines/imines have been replaced with hydrogen in order to reduce computational complexity.

The purpose of this contribution is to investigate whether quantum dynamics simulations, using our newly-developed DD-MCTDH strategy, can provide direct predictive insight of sunscreen function in MAA-like compounds; in other words, we will

This journal is © The Royal Society of Chemistry [year]

investigate whether the predictions of DD-MCTDH simulations align with previous insights into MAA properties obtained from MEP calculations, and to what extent DD-MCTDH can be used to directly correlate molecular structure and sunscreen action. In addition, we note that direct application of DD-MCTDH to the complex molecular species of Fig. 1 remains extremely difficult, even using our DD-MCTDH approach; a key challenge in applying DD-MCTDH to such many-atom molecules is in identifying the set of vibrational coordinates which are essential in describing relaxation and energy dissipation following photoexcitation. To investigate this problem in the context of DD-MCTDH, this Article also proposes and tests a simple computational scheme, based on finding vibrational modes with strong non-adiabatic coupling terms (NACTs) and/or large excited-state forces, to identify the set of active vibrational modes within which DD-MCTDH propagation should be performed.

The remainder of this paper is organised as follows. In Section 2, we first outline the standard MCTDH and DD-MCTDH methods, before describing approaches for identifying an active vibrational coordinate-space within which to perform quantum dynamics, based on projection of excited-state forces and non-adiabatic couplings onto the set of ground-state normal modes. In Section 3, we then highlight the application of DD-MCTDH, along with the newly-proposed active coordinate selection, to study non-adiabatic dynamics in four MAA derivatives. Our quantum dynamics results are analysed in the context of prior computational and experimental work by Losantos and co-workers, with emphasis on direct non-adiabatic quantum dynamics as a route to connecting molecular structure to the rapid non-radiative relaxation, a desirable feature in molecular sunscreens. Disappointingly, we find that our DD-MCTDH simulations cannot reproduce the ultrafast dynamics of the selected model MAAs; however, the underlying reasons for this are explored, and are found to be revealing in pointing the way towards making progress in applying direct quantum dynamics to the correlation of structure and dynamics.

2 Method

In this Section, we outline the key aspects of our computational approach to non-adiabatic quantum dynamics; further details have been published elsewhere.[19–21] In addition, we also discuss simple strategies which can be used to identify a set of vibrational coordinates which might be expected to be important in the non-adiabatic relaxation dynamics of a given molecular systems; such automated coordinate identification methods will be key to the further application of DD-MCTDH to larger molecules.

2.1 DD-MCTDH using a KRR PES

The MCTDH method[1–3] provides a numerically-exact method for solving the TDSE, yielding a time-dependent wavefunction for evaluation of dynamic expectation values and observables such as absorption spectra. The MCTDH method has been, and continues to be, applied to study wavefunction dynamics in a wide range of molecular systems (typically containing a few tens of active degrees-of-freedom), while the development of the multi-layer formulation has pushed the upper limit of system size which is treatable within this framework.[4–6]

Assuming a molecular system with f degrees-of-freedom, the MCTDH wavefunction *ansatz* uses a sum-of-products of basis functions,

$$\begin{aligned}\Psi^{(s)}(Q_1,\cdots,Q_f,t) &= \sum_{j_1=1}^{n_1}\cdots\sum_{j_m=1}^{n_m} A^{(s)}_{j_1,\cdots,j_m}(t)\prod_{\kappa=1}^{m}\varphi^{(s,\kappa)}_{j_\kappa}(Q_\kappa,t) \\ &= \sum_J A^{(s)}_J(t)\,\Phi^{(s)}_J(\mathbf{Q},t)\,.\end{aligned} \tag{1}$$

Here, $\varphi^{(s,\kappa)}_{j_\kappa}(Q_\kappa,t)$ is the j_κ-th basis function on electronic state s and Q_κ indicates the corresponding degree(s)-of-freedom. Each Hartree product $\Phi^{(s)}_J(\mathbf{Q},t)$ is associated with a complex expansion coefficient $A^{(s)}_J(t)$, where we have introduced a compound index, $J=j_1,\cdots,j_f$. At this point, it is worth highlighting the fact that our work on developing direct-dynamics MCTDH schemes has focussed exclusively, to date, on using mass-frequency scaled normal-mode coordinates as the degrees-of-freedom defining molecular configuration space; such coordinates have, so far, been adequate for our simulations, with the added advantage of removing challenges associated with non-diagonal kinetic energy operators. However, we note that our computational approach can, in principle, be generalised to arbitrary coordinate systems.

In MCTDH, the expansion coefficients *and* basis functions are time-dependent; in this way, the number of terms necessary for accurate wavefunction representation can be minimised, enabling treatment of larger system-sizes than more standard grid-based quantum dynamics schemes. Using the Dirac-Frenkel variational principle,[32] one can derive equations-of-motion for the coefficients and time-dependent basis functions (termed single-particle functions [SPFs] in MCTDH terminology). The resulting equations-of-motion, for a system with N_s electronic states, are

$$i\hbar\dot{A}^{(s)}_J = \sum_{u=1}^{N_s}\sum_L \langle\Phi^{(s)}_J|\hat{H}^{(su)}|\Phi^{(u)}_L\rangle A^{(u)}_L, \tag{2a}$$

$$i\hbar\dot{\varphi}^{(s,\kappa)} = \left(1-\hat{P}^{(s,\kappa)}\right)\left(\rho^{(s,\kappa)}\right)^{-1}\sum_{u=1}^{N_s}\langle\hat{H}^{(su)}\rangle^{(\kappa)}\varphi^{(u,\kappa)}. \tag{2b}$$

In Eq. 2b, $\hat{P}^{(s,\kappa)}$ is a projection operator onto the SPF space along mode κ, and $\left(\rho^{(s,\kappa)}\right)^{-1}$ is the inverse of the density matrix associated with κ. The mean-field matrix is given by $\langle\hat{H}^{(su)}\rangle^{(\kappa)}_{jl}=\langle\Psi^{(s,\kappa)}_j|\hat{H}^{(su)}|\Psi^{(u,\kappa)}_l\rangle$, where $\Psi^{(s,\kappa)}_l=\sum_{J^\kappa}A^{(s)}_{J^\kappa_l}\Phi^{(s)}_{J^\kappa}$ defines a single-hole function written in terms of functions $\Phi^{(s)}_{J^\kappa}$, corresponding to SPF Hartree products in all modes apart from κ.

The SPFs, $\varphi^{(s,\kappa)}$, are functions of a small set (1-4) of the degrees-of-freedom in the system, $Q_\kappa=(q_{\kappa_1},\cdots,q_{\kappa_p})$. The SPFs are expanded in a time-independent basis set,

$$\varphi^{(s,\kappa)}_{j_\kappa}(Q_\kappa,t) = \sum_{i_\kappa=1}^{N_\kappa} c^{(s,\kappa,j_\kappa)}_{i_\kappa}(t)\,X^{(\kappa)}_{i_\kappa}(Q_\kappa)\,, \tag{3}$$

with $X_{i_\kappa}^{(\kappa)}(Q_\kappa)$ identifying the i_κ-th basis function for coordinate Q_κ.

A key computational challenge in applying MCTDH lies in evaluating the necessary integrals over the Hamiltonian operator (Eq. 2). When working in rectilinear coordinate systems, as we do here by using vibrational normal-mode coordinates, integrals over kinetic energy operators can be evaluated straightforwardly as one-dimensional terms along each degree-of-freedom. The integrals over the PES, on the other hand, are far from trivial, formally requiring integration over the full f-dimensional space; as a result, a pre-requisite for the *standard* MCTDH algorithm is the availability of a global PES function. In addition, for efficient computation, it is typically required that the global PES function is in the form of a "sum-of-products"; this is a stringent requirement which acts as a roadblock to "on the fly" implementations.

In recent work, we have shown how kernel ridge regression (KRR) can be used to generate a PES in tandem with MCTDH wavefunction propagation; in other words, we have shown how one can achieve direct-dynamics simulations using MCTDH and KRR. In our scheme,[19–21] the PES is given as a weighted-sum of Gaussian kernel functions, with the following form:

$$V(\mathbf{q}) = \sum_{i=1}^{M} w_i k_i(\mathbf{q}_i, \mathbf{q}).$$

As described below, we typically use a set of normal-mode vibrational coordinates $\mathbf{q}$ to describe molecular configuration-space; $\mathbf{q}_i$ is the normal-mode coordinates of KRR reference point i. In our initial work, the kernel functions were chosen to be f-dimensional Gaussian products centred at a set of reference-points $\mathbf{q}_i$, namely

$$k_i(\mathbf{q}_i, \mathbf{q}) = \prod_{j=1}^{f} e^{-\alpha_j (q_i^{(j)} - q^{(j)})^2},$$

where $q_i^{(j)}$ is the value of normal-mode coordinate j for reference point i. Subsequently, we have demonstrated that so-called additive kernels of the form

$$k_i(\mathbf{q}_i, \mathbf{q}) = \sum_{j=1}^{f} e^{-\alpha_j (q_i^{(j)} - q^{(j)})^2} + \sum_{j=1}^{f} \sum_{k=1}^{f} e^{-\alpha_j (q_i^{(j)} - q^{(j)})^2 - \alpha_k (q_i^{(k)} - q^{(k)})^2} + \dots$$

offer a much more computationally-convenient choice of basis function as a result of the increased configuration-space volume associated with each additive kernel function. Regardless of which kernel function is selected, the KRR weights are found by solving a linear system of equations, given by

$$\mathbf{K}\mathbf{w} = \mathbf{b},$$

where $\mathbf{w}$ is the vector of weights, the vector $\mathbf{b}$ contains the set of known PES values evaluated at the reference points (for example, using *ab initio* electronic structure methods),

$$b_i = V(\mathbf{q}_i),$$

and $\mathbf{K}$ is an $M \times M$ covariance matrix (for M reference points) whose elements contain the kernel evaluated for each reference-point pair,

$$K_{ij} = k(\mathbf{q}_i, \mathbf{q}_j) + \gamma^2 \delta_{ij}$$

where γ^2 is a small, positive coefficient used to regularise the matrix. The result of this KRR scheme is the generation of a global PES which is naturally tailored to be more accurate in regions of wavefunction evolution; in addition, the KRR PES generated described above is naturally in the sum-of-products form required for efficient MCTDH simulation. However, we note that further efficiency improvements are possible; for example, we have demonstrated that an additional many-body decomposition of the KRR PES onto the underlying DVR grid of the MCTDH wavefunction results in a much more efficient propagation scheme overall.[21] This approach is used extensively below.

Two important remaining implementation issues relate to the choice of reference points and the adaptation of our scheme to account for non-adiabatic effects. In our DD-MCTDH approach,[19–21] we select KRR reference points based on the natural dynamics of the time-evolving wavefunction, as described previously; here, we generate trial configurations using a uniform sampling function centred on the position expectation value of the time-dependent wavefunction, and with a sufficiently large width to span the relevant region of configuration space. Use of Sobol sequences to select trial geometries within this region ensures an even sampling. At these trial configurations, the variance of the current KRR PES is evaluated. If this variance is larger than a user-defined tolerance, the KRR PES at the selected configuration is judged to be insufficiently accurate and an *ab initio* energy evaluation is performed; the configuration and the corresponding energy are then added to the database of KRR reference points, the KRR weights are updated, and propagation continues. This accept/reject test is performed continually throughout wavefunction propagation (typically every fs), such that the KRR database constantly adapts as new regions of configuration space are explored. At the end of the DD-MCTDH simulation, once a large database of reference points is generated, we usually repeat the dynamics calculation on the KRR PES generated using the full database, without further *ab initio* calculations.

In order to account for non-adiabatic effects, our DD-MCTDH scheme uses one of two different routes to generate diabatic electronic states and energies; we then perform the same KRR fitting scheme described above for each diabatic state (and coupling surface). To date, we have shown that this diabatisation can be achieved using either (i) propagation of an approximate diabatisation matrix using line-integration between nearby points in configuration space,[19,21,33,34] or (ii) by projecting a complete active space self-consistent field (CASSCF) wavefunction expansion onto a reference expansion.[35] We have found so far that these two approaches are equally applicable in DD-MCTDH, but with distinct advantages; for example, the projection diabatisation scheme does not require calculation of non-adiabatic coupling matrix elements, but is less rigorous than the propagation diabatisation. However, in both cases, we have found that calculated dynamic properties are qualitatively similar, and we focus on the projection diabatisation scheme here.

This journal is © The Royal Society of Chemistry [year]

2.2 Selecting active vibrational modes

The discussion of DD-MCTDH above has been predicated on the availability of a set of active vibrational coordinates (or normal modes) which adequately describe the molecular configuration space; but how does one go about choosing the *active* vibrational coordinates *a priori*? For typical organic molecular systems undergoing non-adiabatic dynamics, one might reasonably expect that a few important vibrational coordinates will be most strongly responsible for photo-relaxation, while many other vibrational modes might be simply "spectators", undergoing only simple vibrational motion. Identifying the "active" vibrational coordinates is clearly an important task in successful application of MCTDH; using too many vibrational degrees-of-freedom is computationally-expensive, whereas not using enough might risk "trapping" the time-dependent wavefunction is regions of space from which access to the ground-state becomes hindered.

As a result, several schemes have been proposed to identify active coordinates.[36–38] For example, symmetry considerations are often useful in this regard, and are commonly exploited in MCTDH simulations where relevant, although symmetry is not helpful for complex organic molecules lacking higher-symmetry elements. Identification of active coordinates using classical trajectory simulations has also been proposed and tested successfully, but not in the context of MCTDH. Finally, we note that the approach taken by Lasorne and coworkers,[36] is most similar in spirit to that employed below, focussing on building a simple analytical model which provides orthonormal coordinates pointing along the 'most important' coordinate vectors for ultrafast dynamics; our approach is similar in spirit, but with the ambition to be simpler to implement and avoiding additional PES fitting.

As an alternative step in this direction, we consider here how one might choose a set of active normal-mode coordinates for propagation in DD-MCTDH *without* relying on prior dynamical knowledge or symmetry properties. Our approach can be summarised as follows:

1. We perform a geometry optimization calculation on the ground electronic state, giving a reference geometry $\mathbf{r}_0$,
2. At the reference geometry, we perform a normal-mode analysis, giving the set of ground-state normal-modes, $\{\mathbf{q}_0\}$. From this set of normal-modes, we would like to choose the "active" set which are most likely to be relevant to the subsequent excited-state dynamics.
3. We then calculate the force arising from the *excited-state PES* along each ground-state normal-mode; this is achieved simply using the ground-state normal-mode transformation matrix and the Cartesian forces calculated on the excited-state PES at the Franck-Condon (FC) point;
4. Simultaneously, we calculate the non-adiabatic coupling matrix element between the ground-state and excited-state projected along each of the ground-state normal modes.
5. Finally, from $\{\mathbf{q}_0\}$, we then select the N normal-modes which have either the largest excited-state force components, the largest non-adiabatic coupling components, or both.

The above scheme is clearly motivated by a simply physical picture; those vibrational coordinates which have the largest gradients in the excited-state PES would be expected to be most relevant to dynamics in a 'steepest descent' picture while, at the same time, those coordinates which are most likely to lead towards conical intersections, along strong directions of non-adiabatic coupling, are also most likely to be be essential in capturing the non-adiabatic dynamics.

The advantage of this scheme is clearly it's simplicity; however, it does rely heavily on the underlying idea that the set of ground-state normal-mode coordinates and the available diabatic-states picture are both appropriate to capturing the overall dynamical effects relevant to photodynamics. As we see below, this is often not the case.

3 Application, Results and Discussion

In this Section, we use *ab initio* electronic structure calculations, the DD-MCTDH method described above, and our newly-proposed strategy for selecting dynamically-active vibrational coordinates, to investigate the photodynamics of four MAA-like molecules in an attempt to assess the extent to which wavefunction propagation can be used to predict sunscreen function. We focus here on modelling the molecules shown in Fig. 1; we note that these four molecules are essentially the same as the initial MAA-like molecules investigated by Losantos and co-workers,[28] with the minor change in replacing the methyl groups on the amine/imine moieties with hydrogen atoms. This change is implemented in order to expedite the required *ab initio* electronic structure calculations, and our preliminary investigations indicate that it does not significantly alter the important molecular electronic characteristics which are so vital to photodynamics.

3.1 Single-point energy calculations and coordinate selection

For each of the four molecules considered (Fig. 1), we first performed exploratory CIS calculations using Hartree-Fock natural orbitals. In each case, bright states were located which agreed with the previous work for closely-related MAAs; specifically, initially-excited states were determined as S_2 from molecules 1a and 2a, and S_1 for molecules 3a and 4a. These initial CIS calculations were subsequently used to identify orbital contributions to excited-states in order to define the active space for subsequent CASSCF calculations.

The electronic basis used for molecules 1a and 2a was 6-31G*, and for molecules 3a and 4a it was 6-31G* on carbon and hydrogen, with 6-31+G* on nitrogen and oxygen. A smaller basis was used for molecules 1a/2a due to difficulties with stability in the active space, while for 3a/4a the augmented set was used for O and N as this is usually deemed desirable.

State-averaged-CASSCF (SA-CASSCF) calculations were performed to optimise molecular geometries on S_0. Normal-mode analyses were then performed at the S_0 optimised geometries to generate mass-frequency-scaled normal-mode coordinates for the dynamics calculations. Calculations were also performed at the FC geometries for each molecule to determine forces and Hes-

sians for the bright states, and also to get the non-adiabatic coupling vectors between the bright state and the state immediately below it in energy. Using the normal-modes and frequencies calculated above, the gradients, Hessians and NACTs could be transformed from molecular Cartesian coordinates to mass-frequency scaled normal modes.

We then proceeded to select active vibrational modes for dynamics calculations based on the magnitudes of the forces and NACTs at the FC point in the bright state for each molecules. The results of these simulations are shown in Fig. 2 for molecule 1a. For the modes illustrated, it is clear that there is a range of magnitudes for both the excited-state gradients and the NACTs; in fact, we have only illustrated the largest magnitude normal-modes, with the remainder having negligible contribution. From the gradients, it is clear that some modes have large force contributions in the excited-state, and it is relatively easy to select potentially-active modes from this set. In addition, there are clearly modes which have large NACTs. Perhaps most interesting and useful, it is found that these sets of modes do not necessarily overlap; modes 29-31 would not be selected on the basis of NACTs alone, but are selected once the gradients are also accounted for.

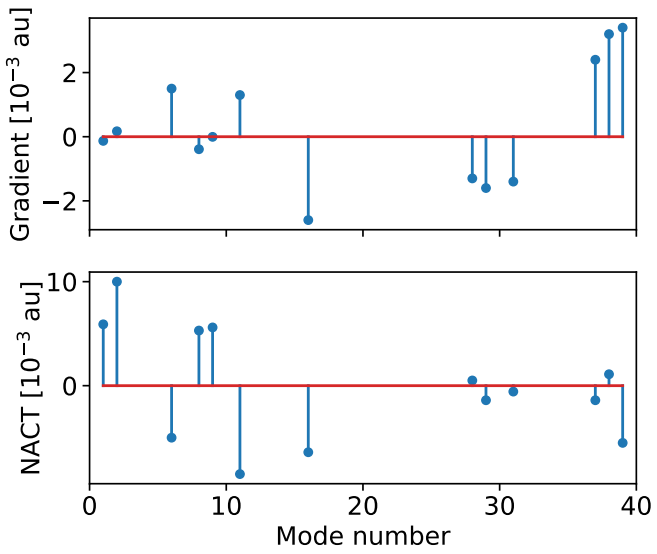

Fig. 2 Excited-state gradients (upper panel) and NACTs (lower panel) for selected ground-state normal-mode numbers for molecule 1a. The lengths of the lines indicate the magnitudes of the forces along each normal-mode in the excited-state, or the NACTs along that normal-mode; in each case, the normal-mode vectors come from geometry optimization and normal-mode analysis on the ground-state.

Based on the gradient and NACT information for each molecule, we selected appropriate normal-modes for subsequent dynamics (see *Supplementary Information*). In addition, we also examined off-diagonal terms in the transformed Hessian in the bright state for each molecule; large absolute values indicate strong coupling between the modes, and strongly-coupled modes were subsequently grouped together in the MCTDH calculations as combined modes to reduce the effort required in the dynamics. By increasing the number of normal-modes which are included for each molecule (*i.e.* by decreasing the threshold on forces and NACTs below which modes are included), we can generate models for MCTDH simulations with increasing complexity in order to test the influence of coupled vibrational modes on the photodynamics.

3.2 MCTDH dynamics simulations

Following identification of sets of active vibrational coordinates for each molecule, we proceeded to set up DD-MCTDH simulations. As a first step, we performed one-dimensional DVR wavepacket propagation simulations for each active vibrational coordinate for each molecule; these simulations were performed to select an appropriate KRR width parameter, as well as identify an appropriate number of DVR basis functions to support the DD-MCTDH wavefunction. With the width parameters and DVR basis set sizes selected, we proceeded to perform f-dimensional dynamics simulations, with increasing numbers of coordinates f for each molecule.

To begin, 6-D DD-MCTDH calculations were run for all four molecules (see *Supplementary information* for details of SPFs, *etc.*); in all cases, the multi-set formulation of MCTDH was used.[2] Initial wavefunctions were taken to be a product of Gaussian functions along each active mode, with width $1/\sqrt{2}$, centred at the FC point on S_2 for 1a/2a and on S_1 for 3a/4a. The default variable mean field integration scheme was used to solve the MCTDH EOMs, employing the Adams-Bashforth-Moulton integrator of order 6, accuracy 10^{-5} and initial step of 10^{-4} fs.

For the generation of the KRR PES, 10^3 molecular geometries *per* state were sampled every 1 fs, within 3 SD of the centres of the wavepackets on each state. These geometries were discarded if the KRR PES variance estimate was below 10^{-3} au. If, instead, the sampled geometries had a variance greater than 10^{-3} au, SA-CASSCF calculations were performed, the resulting energies were diabatised and the results added to the growing KRR PES database. As noted above, to accelerate propagation, a many-body expansion of the KRR PES (truncated at third-order), was employed throughout.

The diabatic state populations for 1a are shown in Fig. 3, as is the absorption spectrum, calculated as the Fourier transform of the wavepacket time-correlation function. Most disappointingly, for molecules 1a, 3a and 4a, we see negligible population transfer from the initially-excited state; the diabatic state populations for 3a and 4a behave in the same way as 1a, and are not shown. In the case of molecules 3a and 4a, rapid transfer to S_0 is expected, as was observed for similar molecules by Losantos and coworkers in both experiments and surface-hopping simulations.[28] In particular, these previous investigations found an excited-state lifetime of 186 ± 49 fs for the methylated version of 3a.

However, for molecule 2a, we do indeed observe population transfer from the initially-excited S_2 state to the S_1 and S_0 states (Fig. 4); this seems to be achieved by a very fast (<20 fs) timescale, followed by a much longer decay, such that relaxation is far from complete after the 100 fs simulation time. Furthermore, the absorption spectrum for 2a is also indicative of ultrafast decay dynamics, with a broad peak with some weaker vibrational peaks

This journal is © The Royal Society of Chemistry [year]

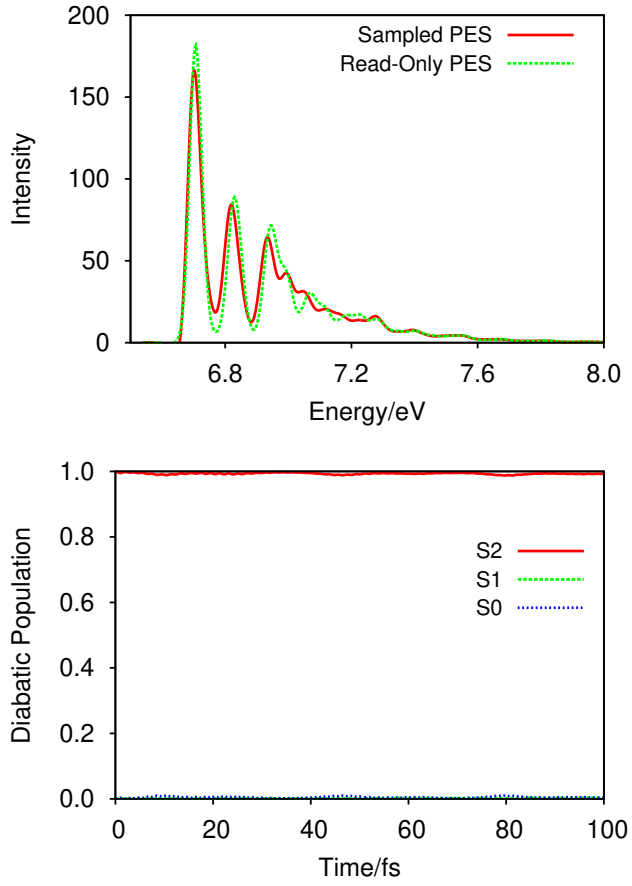

Fig. 3 Upper panel: Absorption spectra of 1a after vertical excitation to the S_2 state, calculated using DD-MCTDH with six normal-modes chosen according to their gradients and non-adiabatic couplings at the FC point. The red, solid line is the result from a calculation with the PES being built on-the-fly whilst the green, dashed line is the result from a second calculation using the pre-computed database to construct the PES. Lower panel: Diabatic state populations from DD-MCTDH simulations calculated on the fully-sampled KRR PES.

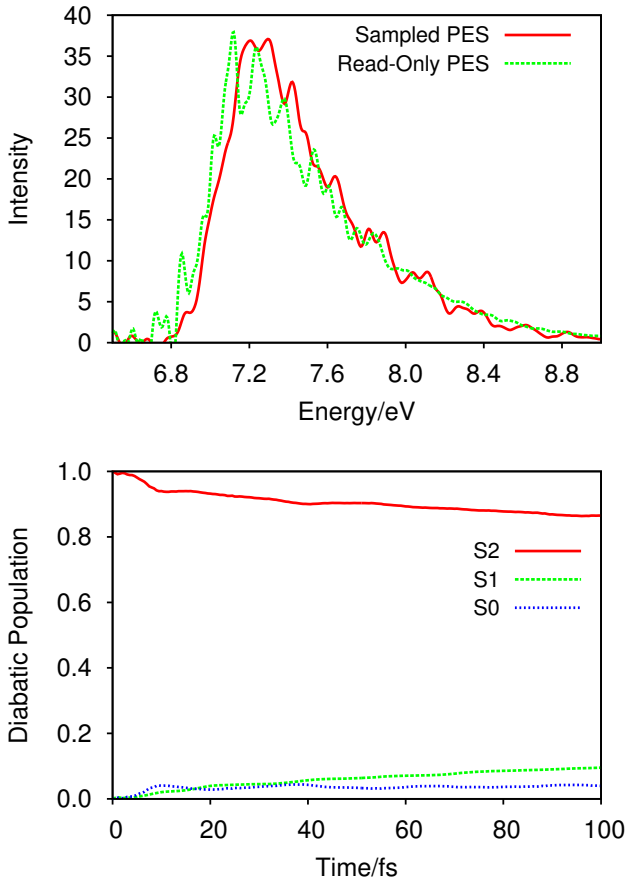

Fig. 4 Upper panel: Absorption spectra of molecule 2a after vertical excitation to the S_2 state, calculated using DD-MCTDH with six normal-modes chosen according to their gradients and non-adiabatic couplings at the FC point. The red, solid line is the result from a calculation with the PES being built on-the-fly whilst the green, dashed line is the result from a second calculation using the pre-computed database to construct the PES. Lower panel: Diabatic state populations from DD-MCTDH simulations calculated on the fully-sampled KRR PES.

superimposed.

Overall, these results are somewhat disappointing; we have performed challenging DD-MCTDH simulations, but we do not observe the expected ultrafast photodynamics for molecules 1a, 3a and 4a. The approach being taken in our simulations and the previous investigations of these molecules are very similar in regards to electronic structure; as a result, we conclude that there are important differences between the dynamics generated by our DD-MCTDH simulations and the previous surface hopping calculations. To assess whether this difference arises due to the reduced dimensionality of our DD-MCTDH calculations (compared to the full-dimensional surface hopping simulations of previous work), we performed a further set of simulations with more active vibrational coordinates. In particular, we have performed additional simulations using 14 active vibrational modes; this represents the largest DD-MCTDH simulations we have performed to date. However, very disappointingly, we found that this made little difference to the dynamics for any of the molecules; in other words, it is not the limited dimensionality of our model systems which is preventing relaxation to the ground-states. There is more to this story, and we believe that the culprits may be the choice of coordinate system and/or the identity of missing diabatic states.

To begin to unravel exactly why we do not see the expected excited-state dynamics in our DD-MCTDH simulations, we focussed on molecule 4a, the smaller of those molecules expected to demonstrate fast decay to the ground-state. To assess whether our choice of normal-mode coordinates was hindering approach to the conical intersection (CI), and hence decay to the ground-state, we modified our choice of normal-mode coordinates in an attempt to drive dynamics towards the CI. First, the optimized geometry of 4a on S_1 and the CI were determined; these calculations found that the S_1 optimized geometry was very close to the CI, and could be reached from a "steepest descent"-like path on S_1. We then tried to find a new set of "pseudo" normal-mode coordinates which are constructed by generating linear combinations of the original set of normal-mode coordinates *plus* additional vectors which connect two or more geometries of interest; the procedure for achieving this is described in the *Supporting In-*

formation. The result of this procedure is a new set of rectilinear normal-mode-like coordinates which contain the original set of normal-mode coordinates, plus additional coordinates which are designed to span the coordinate space connecting the specified geometries of interest; in our simulations, we chose these geometries to be the FC geometry on S_1 and the corresponding CI.

Using this approach, we then performed DD-MCTDH propagation for 1 ps using a 6-D Hamiltonian constructed from the five modes with the largest forces at the FC geometry, plus the additional "pseudo" normal mode connecting the FC geometry on S_1 to the CI. Despite providing a direct coordinate connecting the FC configuration and the CI, we still do not observe ultrafast decay dynamics; in fact, only around 0.2% of the initial S_1 population is transferred to S_0 over the course of 1 ps. Expanding this approach, we then added an additional "pseudo" normal-mode which was designed to connect the FC point to a geometry which was visited during geometry optimization towards the CI on S_1. Again, this additional coordinate gave no further improvement in the predicted excited-state dynamics. Our only conclusion is that the choice of normal-mode coordinates is not significantly hindering excited-state dynamics; when we include additional modes specifically designed to connect key "way-points" along the trajectory from the FC point to the CI, we do not see improvement in the expected dynamics.

Instead, the answer to this problem is suggested in Fig. 5, which shows slices through the diabatic and adiabatic PESs along the "pseudo" normal-mode coordinate connecting the FC point to the CI for molecule 4a. The upper panel in Fig. 5 shows the S_0 and S_1 adiabatic potential energy curves along the "pseudo" normal mode between the FC point (at coordinate $q = 0$) and the CI (seen at around coordinate $q = 21$). Two features are important here: (i) the CI is significantly lower in energy than the S_1 state at the FC point, consistent with the earlier work by Losantos *et al* where the CI was reached very quickly after initial photo-excitation, and (ii) a large energy barrier exists between the FC and CI geometries along this path (around 2.5 eV), suggesting that additional modes must be included for the wavepacket to reach the CI by a barrierless process.

However, the plot in the lower panel of Fig. 5, illustrating the diabatic PESs along the same coordinate as that used to generate the adiabatic PES plots, indicates another problem. The curves in the lower panel of Fig. 5 indicate that the diabatic curves match the adiabatic curves quite closely between the FC point and about coordinate $q \simeq 10$ (*i.e.* approaching the top of the adiabatic barrier). However, beyond this point and towards the CI, the diabatic and adiabatic curves diverge significantly. As the projection diabatisation scheme used here relies on following the configuration interaction expansion vector across configuration space so that a particular diabatic state has a consistent expansion at all geometries, the curves in Fig. 5 indicate that the configuration defining the S_0 and S_1 states at the CI is not included in the reference electronic states selected at the FC point. The implication is that, even by including ever more normal modes in the dynamics calculations, the CI will not be reached because not enough diabatic states have been included to allow the PESs to take the form necessary for the wavepacket to access the CI; the wavepacket is "diabatically trapped" close to the FC point. The projection diabatisation scheme, in principle, allows the inclusion of configurations defined at more than one geometry so that the electronic states near CI could be described correctly; this requires additional work in our dynamics code which has not yet been implemented. However, one encouraging point to note is that the active space natural orbitals correspond closely at both the FC and CI geometries, so the problem is not the "breaking" of the active space. More work will have to be done to resolve this issue.

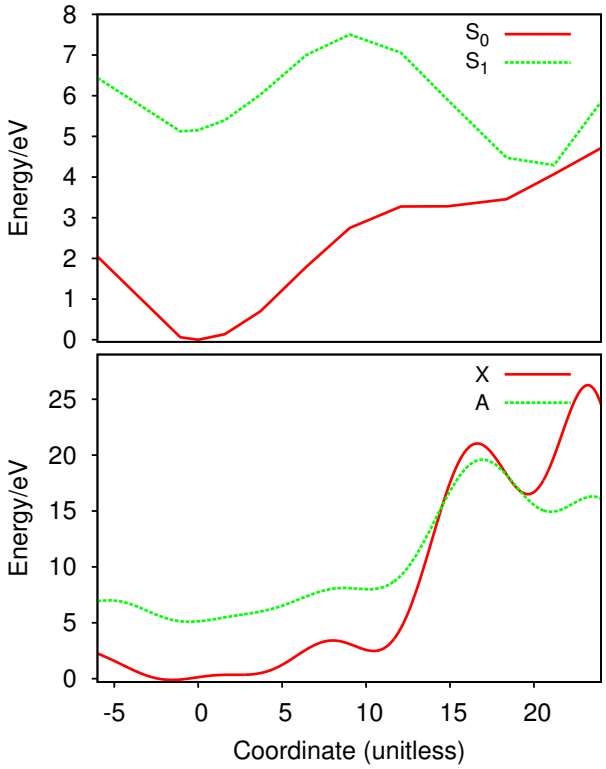

Fig. 5 Upper panel: Adiabatic potential energy curves along the vector between the FC and CI geometries of molecule 4a calculated during a DD-SM wavepacket propagation. The red, solid line is the energy of the S_0 electronic state whilst the green, dashed line is the energy of the S_1 state. Lower panel: Diabatic potential energy curves generated from the adiabatic curves in the upper panel. The red, solid line is the X state which corresponds to the adiabatic S_0 at the FC point whilst the green, dashed line is the A state which corresponds to the S_1 adiabatic state at the same point.

4 Conclusions

On one hand, the conclusions of this paper are somewhat disappointing but, on the other hand, they are very encouraging! We have been able to run direct non-adiabatic wavefunction propagations completely "on-the-fly" using our DD-MCTDH scheme; the ability to run such simulations for systems containing more than 10 degrees-of-freedom is very exciting, and opens up all sorts of possible future applications. However, in the particular examples chosen here, we have found that application of DD-MCTDH was hindered by unanticipated obstacles. Most importantly, we have found that the choice of diabatisation scheme can have a profound effect on the emergent dynamics, to the extent that expected ultrafast decay dynamics is completely absent. We have

This journal is © The Royal Society of Chemistry [year]

rationalised this as arising from a poor choice of diabatic states which were not sufficient to describe the approach towards the CI for our selected molecules, leading to "diabatic trapping".

Fortunately, there is a relatively easy fix - we simply need to adapt our diabatisation scheme so that many more initial adiabatic states are incorporated into our projection scheme for diabatisation. Here, states which may be very high in energy at the FC geometry, but which might become much lower energy at geometries near the CI, could readily be included at little additional cost to the MCTDH propagation; by including these states, the description of the electronic PESs across all sampled geometries would be expected to be much more accurate, and one might anticipate agreement with previous experiments and surface-hopping simulations would emerge. This is ongoing work which should be complete soon, enabling us to then meet our initial goal of connecting sunscreen molecular structure and ultrafast dynamics.

As a final point, we note that further studies performed using the original propagation diabatisation scheme,[19,21,33,34] (as opposed to the projection diabatisation scheme considered here) combined with additional normal-mode-like coordinates as described above, have begun to provide promising results for the ultrafast dynamics of MAAs. A full analysis of these emerging results will be published in due course.

Conflicts of interest

There are no conflicts to declare.

Acknowledgements

We gratefully acknowledge funding from the Leverhulme Trust (RPG-2016-055), the Engineering and Physical Sciences Research Council (EP/R020477/1), and the Energy Global Research Priority at the University of Warwick. We also acknowledge Simon Holland and Vasilios Stavros (University of Warwick) for useful discussions relating to MAA photodynamics.

Notes and references

1 H.-D. Meyer, U. Manthe and L. Cederbaum, *Chem. Phys. Lett.*, 1990, **165**, 73 – 78.

2 M. H. Beck, A. Jäckle, G. A. Worth and H. D. Meyer, *Phys. Rep.*, 2000, **324**, 1–105.

3 *Multidimensional quantum dynamics: MCTDH theory and applications*, ed. H.-D. Meyer, F. Gatti and G. A. Worth, Wiley, Weinheim, Germany, 2009.

4 H. Wang and M. Thoss, *J. Chem. Phys.*, 2003, **119**, 1289–1299.

5 H. Wang, *J. Phys. Chem. A*, 2015, **119**, 7951–7965.

6 O. Vendrell and H.-D. Meyer, *J. Chem. Phys.*, 2011, **134**, 044135/1–16.

7 G. Worth, H.-D. Meyer and L. Cederbaum, *J. Chem. Phys.*, 1996, **105**, 4412–4426.

8 G. Worth, H.-D. Meyer and L. Cederbaum, *J. Chem. Phys.*, 1998, **109**, 3518–3529.

9 A. Raab, G. Worth, H.-D. Meyer and L. Cederbaum, *J. Chem. Phys.*, 1999, **110**, 936–946.

10 S. P. Neville and G. A. Worth, *J. Chem. Phys.*, 2014, **140**, 034317/1–13.

11 G. M. Krishnan and O. Kühn, *Chem. Phys. Lett.*, 2007, **435**, 132–135.

12 J. Li, I. Kondov, H. Wang and M. Thoss, *J. Phys.: Condens. Matter*, 2015, **27**, 134202/1–13.

13 J. Li, H. Wang, P. Persson and M. Thoss, *J. Chem. Phys.*, 2012, **137**, 22A529/1–16.

14 M. Fumanal, E. Gindensperger and C. Daniel, *J. Chem. Theory Comput.*, 2017, **13**, 1293–1306.

15 L. S. Cederbaum, H. Köppel and W. Domcke, *Int. J. Quant. Chem.*, 1981, **15**, 251–267.

16 Q. Meng and H.-D. Meyer, *J. Chem. Phys.*, 2013, **138**, 014313/1–12.

17 M. Fumanal, F. Plasser, S. Mai, C. Daniel and E. Gindensperger, *J. Chem. Phys.*, 2018, **148**, 124119.

18 R. G. McKinlay, J. M. Żurek and M. J. Paterson, *Theoretical and Computational Inorganic Chemistry*, Academic Press, 2010, vol. 62, pp. 351 – 390.

19 G. W. Richings and S. Habershon, *Chem. Phys. Lett.*, 2017, **683**, 228–233.

20 G. W. Richings and S. Habershon, *J. Chem. Theory Comput.*, 2017, **13**, 4012–4024.

21 G. W. Richings and S. Habershon, *J. Chem. Phys.*, 2018, **148**, 134116/1–13.

22 G. W. Richings, C. Robertson and S. Habershon, *J. Chem. Theory Comput.*, 2018, In press, DOI: 10.1021/acs.jctc.8b00819.

23 C. Williams, *Handbook of Brain Theory and Neural Networks*, The MIT Press, Cambridge, Massachusetts, 2002, pp. 466–470.

24 M. A. Collins and D. H. Zhang, *J. Chem. Phys.*, 1999, **111**, 9924–9931.

25 J. Ischtwan and M. A. Collins, *J. Chem. Phys.*, 1994, **100**, 8080–8088.

26 L. A. Baker, S. E. Greenough and V. G. Stavros, *J. Phys. Chem. Lett.*, 2016, **7**, 4655–4665.

27 L. A. Baker, M. D. Horbury, S. E. Greenough, F. Allais, P. S. Walsh, S. Habershon and V. G. Stavros, *J. Phys. Chem. Lett.*, 2016, **7**, 56–61.

28 R. Losantos, I. Funes-Ardoiz, J. Aguilera, E. Herrera-Ceballos, C. García-Iriepa, P. J. Campos and D. Sampedro, *Angew. Chem. Int. Ed.*, 2017, **56**, 2632–2635.

29 J. M. Woolley, M. Staniforth, M. D. Horbury, G. W. Richings, M. Wills and V. G. Stavros, *J. Phys. Chem. Lett.*, 2018, **9**, 3043–3048.

30 W. M. Bandaranayake, *Nat. Prod. Rep.*, 1998, **15**, 159–172.

31 Q. Gao and F. Garcia-Pichel, *Nat. Rev. Microbiol.*, 2011, **9**, 791 EP –.

32 J. Broeckhove, L. Lathouwers, E. Kesteloot and P. Van Leuven, *Chem. Phys. Lett.*, 1988, **149**, 547–550.

33 G. Richings and G. Worth, *J. Phys. Chem. A*, 2015, **119**, 12457–12470.

34 G. W. Richings and G. A. Worth, *Chem. Phys. Lett.*, 2017, **683**, 606–612.

35 C. Robertson, J. Gonzalez-Vazquez, S. Diaz-Tendero, I. Corral and C. Diaz, *J. Comp. Chem.*, 2018, 10.1002/jcc.25764.
36 B. Lasorne, F. Sicilia, M. J. Bearpark, M. A. Robb, G. A. Worth and L. Blancafort, *J. Chem. Phys.*, 2008, **128**, 124307/1–10.
37 S. Manzhos and T. Carrington, *J. Chem. Phys.*, 2008, **129**, 224104/1–8.
38 P. Tavadze, G. A. Franco, P. Ren, X. Wen, Y. Li and J. P. Lewis, *J. Am. Chem. Soc.*, 2018, **140**, 285 – 290.

This journal is © The Royal Society of Chemistry [year]